Study of the Decay $\pi \rightarrow e + \nu$†

E. Di Capua,* R. Garland, L. Pondrom,‡ and A. Strelzoff‡
Columbia University, New York, New York
(Received 16 October 1963)

A large NaI(Tl) crystal has been used to measure the $\pi \rightarrow e/\pi \rightarrow \mu$ branching ratio. From a sample of 10 800 $\pi \rightarrow e$ decay electrons the branching ratio was found to be $R=(1.247\pm0.028)\times10^{-4}$ in agreement with a universal theory for $(e\nu)$ and $(\mu\nu)$ weak couplings.

I. INTRODUCTION

In 1958, Feynman and Gell-Mann[1] and Sudarshan and Marshak[2] independently proposed a universal parity-violating V-A theory of weak interactions, based principally on evidence from nuclear β decay and μ decay. At that time the decay mode $\pi \rightarrow e+\nu$ appeared to be absent. Because the normal pion decay mode is $\pi \rightarrow \mu+\nu$, and because the identity of (e,ν) and (μ,ν) coupling to nucleons was assumed, the absence of $\pi \rightarrow e$ decay was in serious disagreement with the universal theory. Subsequently, $\pi \rightarrow e$ decay was observed,[3,4] and the branching ratio $\pi \rightarrow e\nu/\pi \rightarrow \mu\nu$ was measured to an accuracy of 6%.[5] The ratio was found to be in agreement with the hypothesis of a universal axial vector interaction. Problems remained, however, concerning the strict interchangeability of e and μ in the weak interactions, e.g., the absence of the decay mode $\mu \rightarrow e+\gamma$. An explanation for the absence of this mode has recently been found in the discovery of a muon neutrino distinct from the electron neutrino.[6]

Thus it is now supposed that e and μ are not strictly interchangeable in weak processes, but rather that (e,ν_e) must be interchanged with (μ,ν_μ). This postulate can be accurately tested through a study of the $\pi \rightarrow e\nu/\pi \rightarrow \mu\nu$ branching ratio, which, aside from radiative corrections, depends only on the weak coupling of (e,ν_e) and (μ,ν_μ) to nucleons, and is independent of structure effects due to strong interactions, or due to the existence of a weak intermediate boson. The fact that the muon neutrino resulting from the decay $\pi \rightarrow \mu\nu$ does not produce electrons has therefore stimulated a remeasurement of the branching ratio to 2% accuracy.

The $\pi \rightarrow e/\pi \rightarrow \mu$ ratio, which we shall call R, is of the order of 10^{-4}. Nevertheless, R would be trivial to measure because of the enormous difference in Q value, were it not for the fact that the muon subsequently decays into an electron itself. The energy of the πe electron is 69.8 MeV; the end point energy of the μe electron spectrum is 52.9 MeV. Hence there is a 24% energy difference. In addition, the muon lifetime is 2.2×10^{-6} sec, whereas the pion lifetime is 2.5×10^{-8} sec. Thus the μe electrons can be suppressed by a factor $\sim10^{-2}$ by counting only those electrons emitted within about one-pion lifetime of the time of arrival of the parent pion in the target. In this experiment the necessary energy resolution was achieved with a large NaI(Tl) crystal, and the timing suppression came from a 33 nsec gate in which the electrons were counted. In order to obtain a large πe yield, the 33 nsec time gate began only 4 nsec after the arrival time of the π. The branching ratio was then determined from the number of πe electrons and $\pi\mu e$ electrons counted in the crystal.

II. EXPERIMENTAL PROCEDURE

A. Beam

A source of π^+ mesons at rest was obtained by stopping the 145 MeV/c positive beam from the Nevis synchrocyclotron. This beam contained 80% pions, 10% muons, and 10% positrons. The beam spill was produced by a vibrating target inside the cyclotron. This spill consisted of an early and a late spike, which were electronically excluded from the counting circuitry, and a uniformly populated region about 5.5 msec long. At a repetition rate of 60 cycles, this "gated" spill time gave a duty cycle factor of about 3. The plan view of the scintillation counter configuration is shown in Fig. 1. Counters 1 and 2, $6\times6\times\frac{3}{8}$-in. scintillator, defined the incident beam. Counter 3 was the target in which the pions were stopped, and was $6\times4\times1$ in. inclined at 45° to the beam. A typical (123) coincidence rate with no absorber between counters 2 and 3 was 60 000 per sec. Ten g/cm^2 of CH_2 were placed between 2 and 3 to maximize the stop rate in counter 3. The $123\bar{4}$ stop rate was 30 000 per sec, or one-half of the total beam rate. The distributions of the stopping pion beam in depth in counter 3 and in space across the face of counter 3 were measured for the electron energy loss and muon leakage corrections, to be discussed subsequently. The

† Supported in part by the U. S. Office of Naval Research.
* On leave from the Instituto Nazionale di Fisica Nucleare, Rome, Italy, and the University of Rome, Rome, Italy.
‡ Present address: University of Wisconsin, Madison, Wisconsin.
[1] R. P. Feynman and M. Gell-Mann, Phys. Rev. **109**, 193 (1958).
[2] E. C. G. Sudarshan and R. E. Marshak, *Proceedings of the Padua-Venice Conference on Fundamental Particles, Padua, 1957* (Societa Italiana di Fisica, Bologna, Italy, 1957), p. V-14.
[3] T. Fazzini, G. Fidecaro, A. W. Merrison, H. Paul, and A. V. Tollestrup, Phys. Rev. Letters **1**, 247 (1958).
[4] G. Impeduglia, R. Plano, A. Prodell, N. Samios, M. Schwartz, and J. Steinberger, Phys. Rev. Letters **1**, 249 (1958).
[5] H. L. Anderson, T. Fuji, R. H. Miller, and L. Tau, Phys. Rev. **119**, 2050 (1960).
[6] G. Danby, J. M. Gaillard, K. Goulianos, L. M. Lederman, N. Mistry, M. Schwartz, and J. Steinberger, Phys. Rev. Letters **9**, 36 (1962).

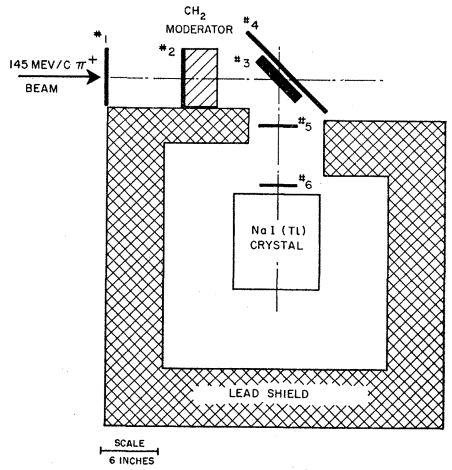

FIG. 1. Plan view of the experimental arrangement. A quadrupole magnet pair was placed immediately to the left upstream. The pions defined by counters 1 and 2 were stopped in counter 3. Counters 5 and 6 defined decay electrons emitted towards the NaI(Tl) crystal.

depth distribution was roughly symmetrical, and had a full width at half-maximum of 2.5 g/cm² of CH_2. The beam was poorly focused after scattering in the CH_2 moderator. The full width at half-maximum was found to be 3 in. for both the horizontal and vertical scans.

B. Electron Telescope

The electron telescope was formed by counters 5 and 6, each 4-in.-diam circles, $\frac{1}{4}$ in. thick. Counter 6 intercepted a fraction 7.25×10^{-3} of a sphere centered at counter 3. The yield of electron coincidences (56) per stop $(123\bar{4})$ was about twice as large as this solid angle predicts, indicating that 50% of the (56) rate was not correlated with a stop in counter 3 but rather with a pion which stopped in the surrounding region. The NaI(Tl) crystal was placed as shown in Fig. 1, on the axis defined by 56, and $\frac{1}{2}$ in. behind counter 6. Electron pulses in the crystal were not required by the fast logic. A $123\bar{4}$ followed by a 56 satisfied the logic, and whatever pulse the NaI crystal produced was stored in a multichannel analyzer.[7] It was found that adding the crystal pulse to the logic did not alter the net electron yield, and complicated the electronics because of the delay of the NaI pulse relative to plastic scintillator. The response of the crystal to electrons in the 50–85-MeV region was measured in a separate experiment, which has been previously reported.[8] The shielding configuration shown was 6 in. thick and 20 in. high, and reduced the low-energy background in the crystal, caused principally by neutrons, to a level such that pile-up effects were negligible.

[7] Supplied by Radiation Instrument Development Laboratories, Melrose Park, Illinois. An external linear gate was used in addition to the analyzer gate to reduce background.

[8] L. Pondrom and A. Strelzoff, Rev. Sci. Instr. **34**, 362 (1963).

C. Fast Logic

A block diagram of the fast logic is shown in Fig. 2. The logic modules were designed by W. LeCroy of Nevis, and employed fast tunnel diodes and transistors. The basic system was capable of rates up to 100 Mc. The general scheme was as follows: a stopping pion in counter 3 produced a $(123\bar{4})$ pulse; a subsequent electron passing through (56) produced a pulse which was then mixed with a delayed $123\bar{4}$ pulse to form $(123\bar{4})(56)$. Four coincidence "boxes" whose time widths were determined by the mixing of $(123\bar{4})$ pulses with (56) pulses were used to measure electrons at early times (πe and $\pi\mu e$ in the "πe box"), electrons at late times ($\pi\mu e$ only in the "long" and "dummy" boxes), and accidentals. Figure 3 gives a sketch of this timing logic. The πe box was placed very close to $t=0$, to maximize the πe yield. The long box was displaced 4 pion lifetimes from $t=0$ to suppress the πe's, and contained only electrons from the $\pi\mu e$ chain. The accidental box was the same length as the long box, and contained electrons which were not physically associated with the corresponding stops. A coincidence in any one of these three channels enabled the NaI crystal output pulse to be stored in one 100-channel group of the analyzer. An open-ended delay line was placed on the input to the discriminator which generated the $(123\bar{4})$ pulse corresponding to the πe box. Two identical pulses were thus made 136 nsec apart for every stop. An electron (56) pulse could then make a coincidence with either one of these stop pulses, in the same coincidence circuit. Which of the two $123\bar{4}$ pulses actually caused the coincidence was then sorted out by subsequent coincidence circuits. The later of these two $(123\bar{4})(56)$ timing boxes was called the "dummy" box. It was not used to trigger the analyzer storage, since a coincidence satisfying the dummy box timing also

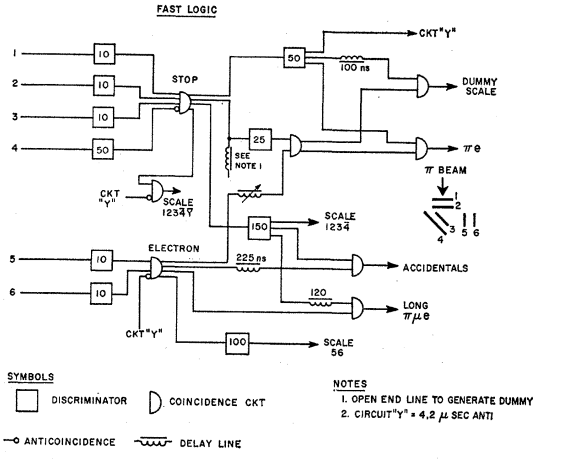

FIG. 2. Block diagram of the fast logic. The length of the output pulse in nsec is written within the discriminator boxes. The purpose of the open ended delay line in generating the dummy box is described in the text.

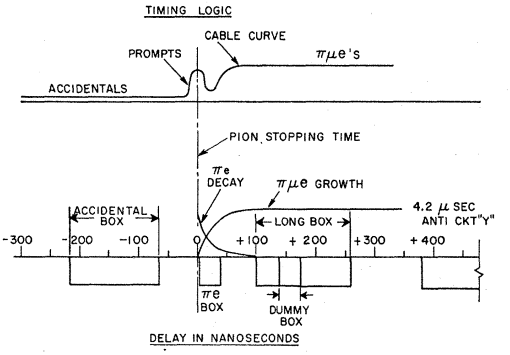

FIG. 3. Sketch of the timing logic sequence. The top drawing is a schematic cable curve, and is not to scale. The relative yields of accidentals, prompts, and $\pi\mu e$'s are approximately correct. The bottom diagram shows the location in time of the various counting boxes. Time zero represents the arrival of the pion in counter 3. The use of the various boxes is discussed in the text.

satisfied the long box timing. The number of dummy counts was recorded on a scaler. Since πe and dummy had precisely the same time width τ_s, the yield of electrons in the dummy box D could be used to eliminate this width from the branching ratio formula. As is shown in Appendix A, the branching ratio R can be written as

$$R=\frac{\lambda_\mu}{\lambda_\pi-\lambda_\mu}\frac{N_{\pi e}}{De^{\lambda_\mu t_s}-N_{\mu e}}(1-e^{-(\lambda_\pi-\lambda_\mu)t_s}), \qquad (1)$$

where $N_{\pi e}$ and $N_{\mu e}$ are the numbers of πe electrons and $\pi\mu e$ electrons in the πe box, and t_s is the separation between the πe box and the dummy box (136 nsec). λ_π and λ_μ are the rates for decay of the pion and muon, respectively. The branching ratio is therefore independent of the solid angle of the electron detector, of the displacement from time zero, and of the width of the time gate in which electrons are counted. The problem of determining $N_{\pi e}$ from the observed crystal spectrum will be considered in Sec. III.

D. Slow Logic

The slow logic is shown in Fig. 4. A timing pulse from the cyclotron triggered the beam gate circuit, which was timed so as to include the uniform part of the vibrating target spill. All output pulses to scalers and the analyzer were in coincidence with the beam gate. Pulses from the πe box, the accidentals box, and the long box addressed the analyzer to the first, third, and fourth block of 100 channels, respectively. Any one of these pulses opened the analyzer gate. Circuit "y" was a 4.2 μsec anticoincidence pulse which prevented an output from the (56) fast logic coincidence circuit after the arrival of a $123\bar{4}$ stop (see Fig. 3). At normal counting rates the action of circuit "y" was to reduce $(123\bar{4})(56)$ accidentals by a factor of 5.

E. Data Collection

The data were collected in 120 runs. Each run consisted of between 10^8 and 2×10^8 stopped pions, lasted for about two hours, and resulted in $\sim$100 πe decay events. The branching ratio was calculated for each run using Eq. (1). Although the branching ratio for each run was not sensitive to drifts in the crystal system or in the timing logic if the equipment was properly adjusted, a periodic monitoring of the behavior of these components was performed. The crystal was viewed by 6 photomultiplier tubes, and the net gain of the system as well as the relative gains of the various tubes varied with time. The position of the edge of the μe electron spectrum served as a gain monitor from run to run. The phototubes were realigned relative to one another about twice a day. The linearity of the crystal-analyzer system was checked by using a variety of low-energy γ sources. This also served to determine the zero shift of the analyzer, which was stable at 10 channels. The stability of t_0, the displacement time between the stop of the π^+ in the target, and the opening of the πe time box, were checked by removing the 10 g/cm^2 of CH_2 between counters 2 and 3, and measuring a delay curve on π^+'s scattered by counter 3 into (56). Such a "prompt" delay curve is shown in Fig. 5. The delay of (56) was normally set at 21 nsec. The timing for electrons and pions was slightly different due to differences in flight time and pulse height in counters 5 and 6, so that this technique did not yield an absolute value for t_0, but rather a check on its constancy. The absolute value of t_0 was eliminated from the measurement of R as in Eq. (1). This curve served a second purpose; it insured that prompt pion events did not trigger the system when the absorber was inserted. Even though most of the $(123\bar{4})$'s represented stops, some of the low-energy pions scattered through 56. The prompt pulse-height spectrum resulting in the

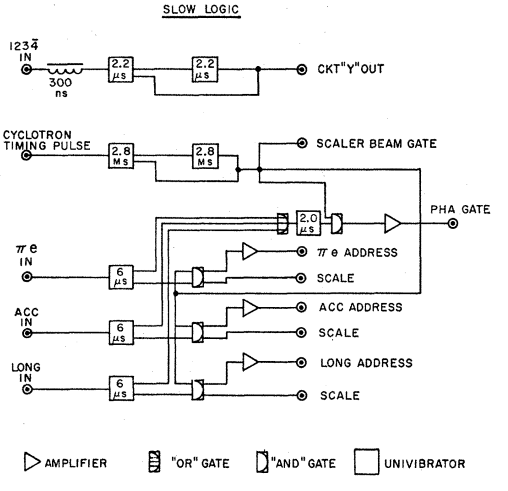

FIG. 4. Block diagram of the slow logic.

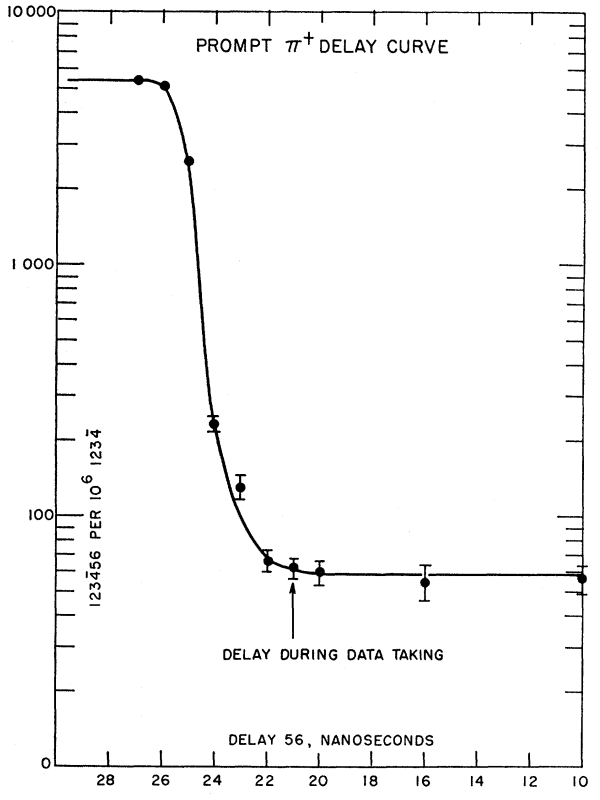

FIG. 5. Prompt delay curve run without the CH_2 moderator between counters 2 and 3. The arrow indicates the normal running delay position, 21 nsec. Increasing the (56) delay moved the window closer to "time zero." Note that at 21 nsec all of the prompts were accidentals, and hence were removed by the accidentals subtraction.

crystal from these scattering events was easily measured, and delay curves such as Fig. 5 insured that, under normal conditions, the prompt contamination of the πe box was $\lesssim 0.5\%$ of the total number of πe's. The long and accidentals boxes were supposed to have the same width τ_L, and of course it was essential that the πe box and the dummy box had the same width. These gate widths were measured between data runs by triggering (123$\bar{4}$) at random, and driving (56) by a 1 Mc crystal oscillator. Thus, 1000 counts in (123$\bar{4}$56) for 10^6 random (123$\bar{4}$)'s represents a box width of 1 nsec. The identity of the widths of the πe and dummy boxes could be checked in a few minutes to a statistical error of ± 0.1 nsec.

III. DATA ANALYSIS

The total multichannel analyzer spectrum obtained after accidentals subtraction in the πe time box is shown in Fig. 6. This spectrum was calculated by correcting for gain variations, and summing channel by channel all of the πe time box spectra collected in the 120 separate runs. Similarly, the total pure ρ spectrum from the long box is plotted in Fig. 7. The total accidentals spectrum was found to be similar to Fig. 7, that is, the accidentals were all $\mu \rightarrow e$ electrons. The energy resolution in the accidentals spectrum was somewhat poorer, however, due to the "uncorrelated" accidentals which came from a source more extended in space than counter 3.

As is clear from Fig. 6, the NaI crystal resolution was not sufficient to separate the πe peak clearly from the $\pi\mu e$ continuum. The number $N_{\pi e}$ in Eq. (1) could not be obtained by summing the raw data, but had to be corrected first for the number of $\pi\mu e$'s in the neighborhood of the πe peak (a correction effected by using the spectrum of Fig. 7), and second for a missing "tail" which was lost under the $\pi\mu e$ continuum due to the NaI resolution function. The data obtained in the crystal calibration experiment were used for the tail correction.

By normalizing the ρ spectrum of Fig. 7 to the pure $\mu \rightarrow e$ part of Fig. 6 and subtracting channel by channel, the crosses in Fig. 6 were obtained. These crosses represent the pure $\pi \rightarrow e$ contribution. Figure 8 shows the upper end of this spectrum. All three of these figures show a periodic decimal distortion due to a channel addressing error. No effort was made to remove this error from the data, although during the experiment tests were made which showed that no loss of counts

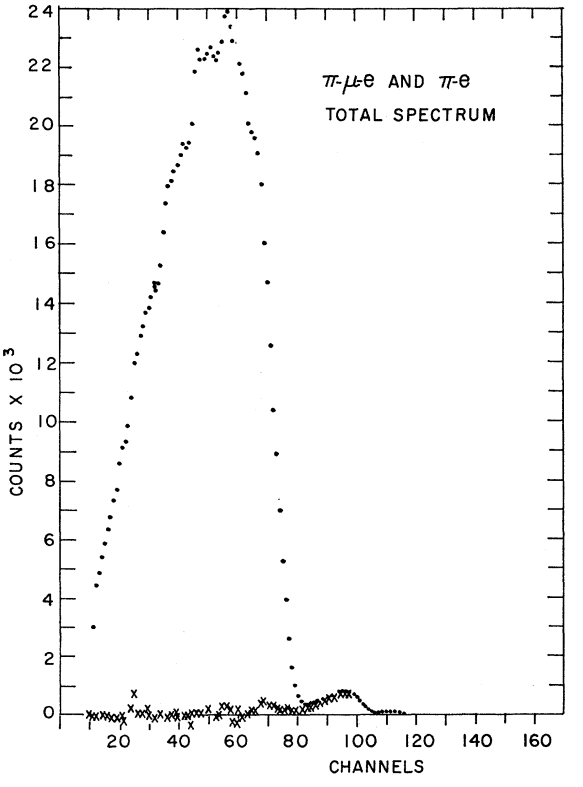

FIG. 6. Total pulse-height spectrum for all of the runs obtained in the πe time box. The abscissa has been corrected for analyzer zero shift. The crosses resulted when the pure μe spectrum was subtracted off.

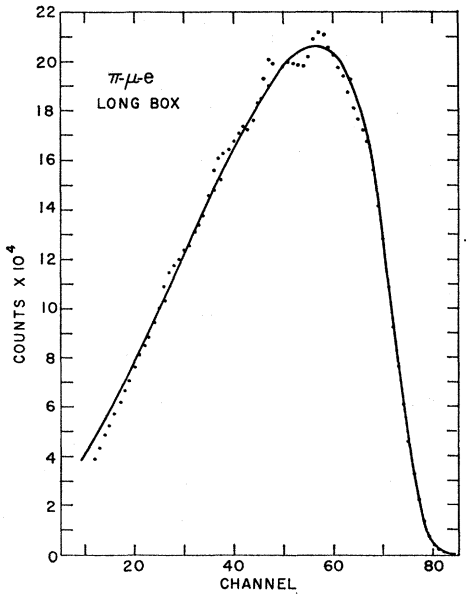

FIG. 7. Total pure μe ρ spectrum from the long box. The abscissa has been corrected for analyzer zero shift. The periodic distortion was due to an analyzer addressing error. The solid curve was calculated assuming $\rho = \frac{3}{4}$ and a crystal resolution of 15%. Note a small indication of an energy-dependent electron efficiency for the counting system at very low-electron energies.

was involved in the distortion. A typical calibration run from Ref. 8 is shown in Fig. 9. The crystal response function was found to be asymmetrical, and characterized by a long low-energy tail. Small changes in the width of this function due to symmetrical broadening such as energy spread from the target had little effect on the low-energy tail. The πe peak and the $\pi\mu e$ spectrum were fitted simultaneously with a resolution curve 15.3% wide, corresponding to an 8% wide Gaussian

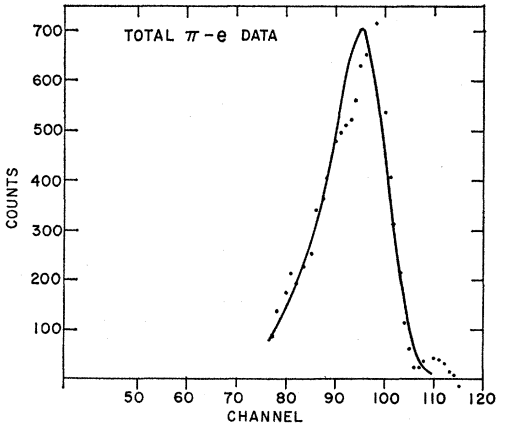

FIG. 8. Expanded plot of the πe spectrum. Channel 78 represents the energy where the cut was made, as discussed in the text. Note that the analyzer distortion has shifted the peak somewhat, but the sides of the curve fit the data very well. This fit and the fit of Fig. 7 were made simultaneously and of course the energy difference between the two curves is constrained by kinematics.

for the stopping distribution folded in to the 13.5%-wide resolution function of Fig. 9. This result was consistent with the energy spread due to the stopping distribution. The solid curves in Figs. 7 and 8 represent this fit. Channel 78 in Fig. 8 represents the energy cutoff. The fraction of counts in the tail below this cutoff was 9.1%. To this number a statistical error of $\pm 0.5\%$ from the calibration data, and a systematic error $\pm 0.5\%$ due to uncertainty in this fit were assigned. It is also clear from Fig. 7 that the very low-energy $\mu \rightarrow e$ electrons were lost from the ρ spectrum. This correction amounted to 3.7% with an assigned $\pm 0.3\%$ systematic error.

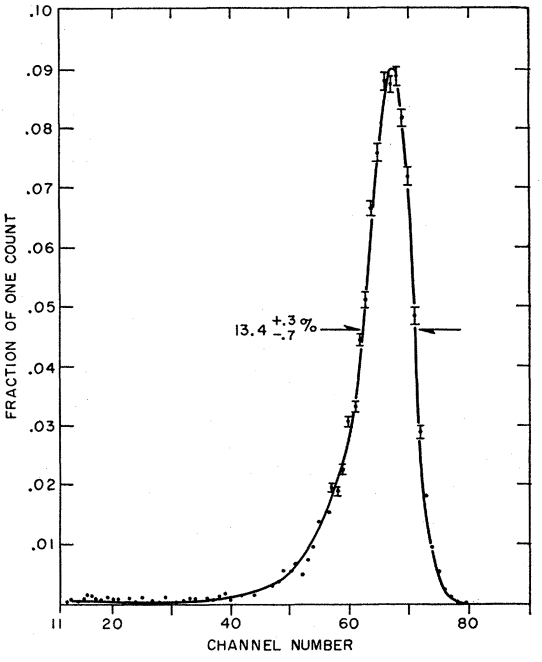

FIG. 9. A typical calibration curve from Ref. 8.

After the total spectra had been studied to determine the tail corrections, the branching ratio could be calculated with Eq. (1) for each run. The calculation of R for an individual run proceeded in the following way: first the pulse-height spectra in the πe box and the long box were corrected for accidentals, using the spectrum in the accidentals box; then the $\mu \rightarrow e$ spectrum in the long box was properly normalized and subtracted channel by channel from the πe box spectrum to yield the pure πe spectrum; the πe spectrum was then summed beginning with the channel nearest to channel 78 in Fig. 8, and the tail fraction was corrected for the small difference in energy; finally, the number of dummy counts from the scaler, corrected for accidentals, was combined with the number of $\pi\mu e$ counts from the analyzer, and R was calculated using the appropriate tail corrections and separation time between the dummy and πe boxes. Table I illustrates typical data

TABLE I. Typical data from a single run. For an explanation of the calculations, see Appendix B.

(A) Scaler data

Total stops	133×10^6
Dummy	18 754
Long	87 801
Accidental	12 231
N_{LONG}'	75 570
D'	16 209

(B) Pulse-height analyzer data

	SUM Ch 1–68	SUM Ch 78–120	SUM Ch 1–120
LONG	77 273	471	81943
ACC	9405	90	9973
πe box	9639	152	10224
N_{LONG}'	67 868	381	71970
$N_{\pi\mu e}'$	7669	133	...
$N_{\pi e}'$	...	90	...

for a single run. The details of the calculation presented in this table are discussed in Appendix B. This operation was written in a FORTRAN program and performed on the IBM 7090 at the Columbia Computing Center. In addition, the program calculated the statistical error for each run, and kept a weighted average value of R and a total error talley as each successive run was analyzed. Figure 10 shows the scatterer of R values for the runs, the typical statistical errors, and the weighted mean value.

The final calculated value of R was 1.251×10^{-4} with a statistical error of $\pm1.3\%$. The total number of summed πe counts was 10 891. The $\pi\mu e-\pi e$ subtraction process increased the statistical error somewhat. This value was lowered by 0.3% by correcting for muons which left the target counter and were therefore unavailable for $\pi\mu e$ decay events. This number was derived from the known pion stopping distribution and the range of the muon. As is shown in the Appendix, the use of the dummy box eliminated the effect of muons in the beam which stopped in counter 3. Table II shows the final value for R, and the various sources of systematic and statistical error involved. The systematic errors were added algebraically and then combined in quadrature with the statistical error and the error in the pion lifetime to give a total error of $\pm2.2\%$, or $R=(1.247\pm0.028)\times10^{-4}$.

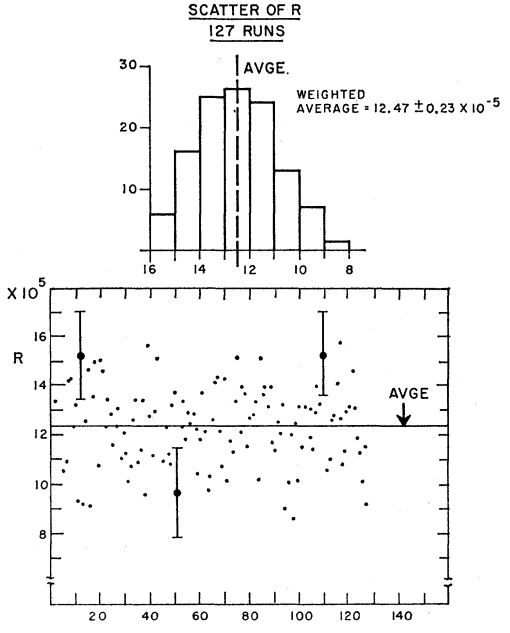

FIG. 10. Scatter diagram for the ratio values calculated from each of the runs. Typical statistical errors and the final value are shown.

TABLE II. Final branching ratio and the various statistical and systematic errors. The quantities f, g, τ_π, and the muon loss correction are factors occurring in the expression for R.[a]

Quantity	Value	Statistical error	Systematic error
R	1.247×10^{-4}	1.3%[b]	...
muon loss	0.997		0.5%
g	1.091	0.5%[c]	0.5%
f	1.037		0.3%

[a] Total systematic error = 1.3%; total statistical error = 1.4%; total assigned error = 2.2% including 1.2 error in τ_π (Ref. 13).
[b] Counting statistics on 10,800 πe's, including $\pi\mu e$ subtraction error.
[c] Error due to uncertainties in experimentally observed πe shape.

IV. DISCUSSION

The $\pi e/\pi\mu$ branching ratio predicted by a theory which assumes equal axial vector coupling constants for (e,ν) and (μ,ν) is

$$R=\left(\frac{m_e}{m_\mu}\right)^2\left(\frac{m_\pi^2-m_e^2}{m_\pi^2-m_\mu^2}\right)^2. \tag{2}$$

Using the most recent mass values, this formula yields

$$R=1.282\times10^{-4} \tag{3}$$

if no account is taken of the radiative corrections. In this experiment both $\pi\rightarrow e+\nu$ and $\pi\rightarrow e+\nu+\gamma$ were measured, because the bremsstrahlung, being sharply peaked at small angles with respect to the electron, accompanied the electron into the crystal, and the total energy deposited was therefore (E_e+E_γ) with high probability. Hence, the desired theoretical branching ratio is $R=[(\pi\rightarrow e+\nu)+(\pi\rightarrow e+\nu+\gamma)]/(\pi\rightarrow\mu+\nu)$. Kinoshita[9] has calculated this ratio. He expressed the correction term, which lowers the predicted value of R, in two parts. One part comes from renormalization effects in which no real photons come out, and the other part comes from $\pi\rightarrow e+\nu+\gamma$. The total correction

[9] T. Kinoshita, Phys. Rev. Letters 2, 477 (1959). See also S. Berman, Phys. Rev. Letters 1, 468 (1958).

amounts to -3.9%, yielding

$$R_{\text{th}}=1.232\times10^{-4}, \tag{4}$$

which is to be compared with the result of this experiment. The difference $R_{\text{exp}}-R_{\text{th}}=0.015\times10^{-4}$ is within one-half standard deviation of the experimental result. This result is, therefore, in agreement with the universal theory. No difference between (e,ν_e) and (μ,ν_μ) coupling has been found.

The sensitivity of this experiment to two effects of current interest should be mentioned. The weak intermediate boson, if it exists, can effect R only through the radiative corrections. The contribution of a boson has been calculated by Shaffer,[10] who finds terms of the order $(m_\pi/m_w)^2$ in the radiative correction formula. This quantity at present seems to be $\sim10^{-2}$, and is thus a very small part of the radiative corrections.[11] The muon neutrino can have properties distinct from the electron neutrino, as discussed by Friedberg.[12] Writing the $(\mu\nu)$ term in the Lagrangian as

$$\bar{\psi}_\mu\gamma_\lambda[(1+\gamma_5)+a(1-\gamma_5)]\psi_\nu,$$

and allowing for $m_\nu\neq0$, one finds the branching ratio $R=R_0[1+2.78a(m_\nu m_\mu/E_\nu E_\mu)]$. From this experiment we have $2.78a(m_\nu m_\mu/E_\nu E_\mu)=0.015\pm0.028$, and, therefore, $am_\nu=(0.16\pm0.31)$ MeV.

ACKNOWLEDGMENTS

This experiment could not have been performed without the cooperation of the Nevis staff. Professor Leon Lederman gave continual advice and encouragement. Walter Le Croy designed and built the electronic logic. The cyclotron crew under William Hunt maintained the machine in peak order for the final data runs. Stimulating discussions were had with Dr. Sheldon Penman during the early stages of the work. One of us (E.DiC.) wishes to thank Professor Lederman for the hospitality extended to him at Nevis.

APPENDIX A: DERIVATION OF BRANCHING RATIO FORMULA

The number of πe electrons counted in a time box of width τ, beginning a time t_0 after the arrival of the pion, is given by

$$N_{\pi e}=RN_\pi\Omega e^{-\lambda_\pi t_0}(1-e^{-\lambda_\pi\tau}), \tag{A1}$$

where R is the $\pi\to e/\pi\to\mu$ branching ratio, $N_\pi\Omega$ is the number of pions times the solid angle, and λ_π is the pion decay rate. The number of $\pi\mu e$ electrons counted in this same box is

$$N_{\pi\mu e}=N_\pi\Omega\frac{\lambda_\pi\lambda_\mu}{\lambda_\pi-\lambda_\mu}\left\{(1+f)\frac{e^{-\lambda_\mu t_0}}{\lambda_\mu}(1-e^{-\lambda_\mu\tau})-\frac{e^{-\lambda_\pi t_0}}{\lambda_\pi}(1-e^{-\lambda_\pi\tau})\right\}, \tag{A2}$$

where λ_μ is the muon decay rate, and f allows for a fraction of the stop triggers to be muons rather than pions. In this experiment, f was of the order of 1% due to pion decay in flight after the absorber, and muons of lower energy in the beam. Similarly the number of μe electrons counted in the dummy box, separated from the πe box by t_s, is given by

$$D=\frac{N_\pi\Omega\lambda_\pi\lambda_\mu}{\lambda_\pi-\lambda_\mu}\left\{(1+f)\frac{e^{-\lambda_\mu(t_s+t_0)}}{\lambda_\mu}(1-e^{-\lambda_\mu\tau})-\frac{e^{-\lambda_\pi(t_s+t_0)}}{\lambda_\pi}(1-e^{-\lambda_\pi\tau})\right\}. \tag{A3}$$

Thus defining coefficients A and B which depend on $N_\pi\Omega$, t_0 and τ as follows:

$$\begin{aligned}A&=N_\pi\Omega\frac{\lambda_\mu}{\lambda_\pi-\lambda_\mu}e^{-\lambda_\pi t_0}(1-e^{-\lambda_\pi\tau}),\\ B&=N_\pi\Omega(1+f)\frac{\lambda_\pi}{\lambda_\pi-\lambda_\mu}e^{-\lambda_\mu t_0}(1-e^{-\lambda_\mu\tau}),\end{aligned} \tag{A4}$$

we see that

$$\begin{aligned}N_{\pi\mu e}&=B-A,\\ D&=(e^{-\lambda_\mu t_s})B-(e^{-\lambda_\pi t_s})A,\end{aligned} \tag{A5}$$

and

$$N_{\pi e}=R\left(\frac{\lambda_\pi-\lambda_\mu}{\lambda_\mu}\right)A. \tag{A6}$$

Equations (A5) can be solved for A, which, when substituted into Eq. (A6) yields

$$R=\frac{\lambda_\mu}{\lambda_\pi-\lambda_\mu}\frac{N_{\pi e}}{e^{\lambda_\mu t_s}D-N_{\pi\mu e}}(1-e^{-(\lambda_\pi-\lambda_\mu)t_s}), \tag{A7}$$

which is Eq. (1). It is interesting to note that the possible muon contamination of the stopping beam drops out of the formula.

APPENDIX B: SAMPLE NUMERICAL CALCULATION

This Appendix explains Table I. If we assume that the pion lifetime is 25.5 nsec,[13] then Eq. (1) can be written for computation as

$$R=(0.01167)(g/f)N_{\pi e}'/(1.067\epsilon D'-\beta N_{\text{LONG}}'), \tag{B1}$$

where the first numerical factor is the lifetime ratio, and the second is $\exp(\lambda_\mu\pi_s)$; g and f are tail corrections; primes indicate correction for accidentals;

$$\epsilon=(N_{\text{LONG}}')_{\text{PHA}}/(N_{\text{LONG}}')_{\text{SCALER}}$$

corrects for the pulse-height analyzer loss, and $\beta=N_{\pi\mu e}'/N_{\text{LONG}}'$ normalizes the pure ρ spectrum to

[10] R. A. Shaffer, Phys. Rev. **131**, 2203 (1963).
[11] H. Faissner, Bull. Am. Phys. Soc. **8**, 466 (1963).
[12] R. Friedberg, Phys. Rev. **129**, 2298 (1963).
[13] J. Ashkin, T. Fazzini, G. Fidecaro, Y. Goldschmidt-Clermont, N. Lipman, A. Merrison, and H. Paul, Nuovo Cimento **16**, 490 (1960).

the first (πe) time box. In calculating β, the spectra in Table I were summed only to channel 68, thus omitting the πe peak. Assuming that the fraction of accidentals was strictly proportional to the width of the time gate, we have

$$N_{\mathrm{LONG}}'=N_{\mathrm{LONG}}-\mathrm{ACC}, \tag{B2}$$

and

$$D'=D/(1+0.978(\mathrm{ACC}/N_{\mathrm{LONG}}')). \tag{B3}$$

Similarly, in the πe box,

$$N_{\pi\mu e}'=N_{\pi\mu e}-0.978(D'/N_{\mathrm{LONG}}')\mathrm{ACC}. \tag{B4}$$

Using only the data from channels 78–120, $N_{\pi e}'$ is given by

$$N_{\pi e}'=N_{\pi\mu e}'-\beta N_{\mathrm{LONG}}'. \tag{B5}$$

Now from the data in Table I we find

$$\epsilon=0.952,\quad \beta=0.113,$$
$$1.067\epsilon D'-\beta N_{\mathrm{LONG}}'=16404-8130=8274.$$

Taking $g=1.091$ and $f=1.037$, we obtain

$$R=(1.33\pm0.17)\times10^{-4}.$$

PHYSICAL REVIEW VOLUME 133, NUMBER 5B 9 MARCH 1964

Fairly Low-Energy Pion-Pion Scattering. II*

ALVIN M. SAPERSTEIN† AND JACK L. URETSKY
Argonne National Laboratory, Argonne, Illinois

(Received 16 October 1963)

We have extended the pion-pion calculation of Smith and Uretsky by including the third-order perturbation theoretic terms for the discontinuity across the left-hand cut in the complex energy plane. The right-hand cut is still given by elastic unitarity. Numerical calculations for the S- and P-wave amplitudes show that the S waves are not much different than they were in the second-order calculation. The P-wave amplitude is substantially modified, and the trends are such as to make it plausible that a fourth-order calculation could reproduce the ρ resonance. It was also interesting to find that the P-wave interaction can be strongly attractive (to this order) only if the S-wave interactions are repulsive.

I. INTRODUCTION

IN an attempt to formulate a theory of pion-pion scattering it was shown, in an earlier paper,[1] how one could define a sort of generalized potential to describe the π-π interaction and then make use of dispersion-theoretic methods to obtain the scattering from this "potential." The generalized potential is calculated by means of field-theoretic perturbation theory as a power-series expansion in a "renormalized" coupling constant λ that specifies the strength of a $\lambda\phi^4$ interaction among the pions. In paper I the potential was calculated to order λ^2 and the solutions were described and discussed. The present paper is devoted to a discussion of the consequences of including the λ^3 term in the "potential." We hope to be able to discuss the fourth-order corrections in the near future.

It seems appropriate to recount the conditions that should be fulfilled by the calculations we are doing in order that they may correspond to a sensible theory. Relativistic invariance and unitarity of the scattering amplitude require no discussion, of course, since these are built into the computational method. One also desires to impose crossing symmetry, and it was pointed out in I that this cannot be precisely defined in a calculation such as ours of partial-wave amplitudes. It was found that an approximate crossing symmetry was quite well maintained for not too large values of the coupling constant λ.

One other important condition having to do with the convergence of the method was given passing mention in paper I. The hope was expressed there that the effect of including higher order terms in the potential would correspond to working one's way "outward" in both angular momentum l and energy E. This notion is expressed graphically in Fig. 1 which is a sketch of the $l-E$ plane. There is a point in this plane (labeled "A") where the lowest order expression (proportional to λ) for the scattering amplitude is exact. Around this must be a zone (labeled "B") where the second-order calculation contained in paper I is a good approximation. In

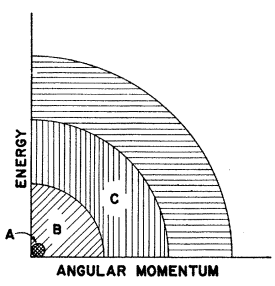

FIG. 1. Sketch of the expected regions of applicability of the different orders of approximation. For explanation see text. The units are, of course, arbitrary.

* Work performed under the auspices of the U. S. Atomic Energy Commission.

† Permanent address: Department of Physics, Wayne State University, Detroit, Michigan.

[1] K. Smith and J. L. Uretsky, Phys. Rev. **131**, 861 (1963). This will be referred to as paper I.